Detection of potentially gas flaring related pollution on vegetation cover and its health using remotely sensed data in the Niger delta, Nigeria

Barnabas O. Morakinyo[1,2,3,4]⊠
Samantha Lavender[2,3]
Victor Abbott[2]

(⊠ Corresponding Author)

[1]*Department of Surveying & Geoinformatics, Faculty of Environmental Sciences, BAZE University, Abuja, Nigeria.*
[2]*School of Marine Science & Engineering, Faculty of Science & Technology, University of Plymouth, Plymouth, UK.*
[3]*Pixalytics Ltd, Plymouth, UK.*
[4]*ARGANS Ltd, Plymouth, UK.*
[1,2,3,4]*Email: barnabas.ojo@bazeuniversity.edu.ng*
[2,3]*Email: Smnthlavender@gmail.com*
[2]*Email: Jamesvictor2021A@gmail.com*

Abstract

Detection of potentially gas flaring-related pollution on vegetation cover using remotely sensed data at 11 flaring sites in Rivers State, Nigeria is the emphasis of this research. 21 Landsat 7 Enhanced Thematic Mapper Plus (ETM+), and 4 Landsat 8 Operational Land Imager and Thermal Infrared Sensor (OLI-TIRS) data dated from 21/04/2000 to 05/02/2022 with < 3 % cloud cover were used. Normalized Differential Vegetation Index (NDVI) was retrieved from corrected Landsat 7 bands (1-4), and Landsat 8 bands (2-5). Corrected thermal band was used for the computation of Land Surface Temperature (LST). Change in NDVI $(\delta NDVI_{450-60})_m$ and LST $(\delta LST_{60-450m})$ were computed. NDVI values at 60 m from the stack show that as the year increases, NDVI values around the stack reduces to almost zero. Linear regression analysis was considered for $(\delta NDVI_{450-60})_m N$ against $(\delta NDVI_{450-60})_m E$, $(\delta NDVI_{450-60})_m N$ against $(\delta NDVI_{450-60})_m S$, and $(\delta NDVI_{450-60})_m N$ against $(\delta NDVI_{450-60})_m W$. Only $(\delta NDVI_{450-60})_m N$ against $(\delta NDVI_{450-60})_m W$ give statistically significant results at 99 % confidence level (p-value = 0.0016). $(\delta NDVI_{450-60})_m N,E,S,W$ against $(\delta LST_{60-450})_m N,E,S,W$ were considered and results show positive correlation but statistically insignificant. Based on the results of this research, it can be concluded that flaring-related pollution can be detected on vegetation cover using Landsat 7 and Landsat 8 data in the Niger Delta.

Keywords: Detection, Landsat 7, Landsat 8, Niger delta, Pollution, Remotely sensed data, Vegetation cover.

Contents

Contribution of this paper to the literature
This study contributes scientific knowledge on detection of potentially gas flaring-related pollution on the vegetation cover and its health using Earth Observation (EO) Satellite data.

1. Introduction

Extraction and processing of crude oil and natural gas in the Niger Delta have unfavourable and harmful effects on the environment [1-4]. Oil spillage and gas flaring alter the attributes of the receiving environment, leading to its pollution and degradation [1-4]. Among others, gas flaring is responsible for the contamination of vegetation in the Niger Delta [5] with destructive impacts on vegetation and agricultural pursuits [6]. For example, almost no vegetation grows in the area directly surrounded by the flare as a result of the tremendous Carbon emissions and heat releases to the environment; and the acidic nature of the soil potential of Hydrogen (pH) [2].

Researchers have worked on gas flaring with different aims and methods internationally, for example [7] used Sentinel-3A Sea and Land Surface Temperature Radiometer (SLSTR) data to study flared gas volume and emission of black carbon globally. The impact of Hydrogen Sulphide (H_2S) content and excess air on pollutant discharges at the 2 flare sites in Iran using computational methodology with Matrix Laboratory (MATLAB) codes was examined by Zoeir, et al. [8]. They stated that the impact of Sulphur III Oxide (SO_3) is several times more destructive than that of Sulphur II Oxide (SO_2) in acidic rains; and that Sulphur III Oxide (SO_3) pass through a slow balance with water vapour available in the atmosphere and forms Sulphuric acid (H_2SO_4). H_2SO_4 is a highly corrosive compound within acidic rains. Acidic rain affects soil pH which in turn causes destruction of vegetation and plants. Others studies on global gas flares includes atmospheric pollution [9, 10] and estimation of temperatures of vegetation fires [11] etc.

In Nigeria, some studies have been carried out regarding discharge of gas flare activities; and its effects on the environment and people. In the Niger Delta, Ndinwa, et al. [6] used questionnaire to study the impacts of flared gas on the environment and health of the people of Kwale communities, Ndokwa West Local Government Area. Chukwu, et al. [12] and Uyigue and Enujekwu [13] adopted conventional methods by taking measurements on site using instruments, and collection of samples to study gas flaring impacts at 2 communities of Mkpanak and Iko, Ibeno and Eastern Obolo Local Government Areas respectively, Akwa Ibom State. The influence of flared gas on vegetation and water resources for the entire Niger Delta region was reviewed by Seiyaboh and Izah [14]. Lawanson, et al. [15] worked on the consequences of gas flaring on the cassava plantations in the Niger Delta. Such effects recorded on vegetation and agricultural activities includes deforestation [16] stunted growth of crops [6, 12] reduction of soil quality parameters [17] etc. The authors concluded that the comparison between the flaring and the control sites used for their researches show that the soil nutrients of the flaring sites were the lower. In addition, Chukwu, et al. [12] recorded the influence of flared gas on plants and vegetation as the loss of leaves at a distance less than 1 km, withering (1-2 km), stunted growth (3-4 km), and wrinkling leaves (5-6 km) respectively from the flare stack. However, none of the existing studies on flared gas and its consequences/impacts on vegetation in the Niger Delta has used satellite data.

Furthermore, many scholars investigated the relationship between the Normalized Differential Vegetation Index (NDVI) and Land Surface Temperature (LST) using different satellite data [18-26]. For example, Allam, et al. [18] worked on the effect of land surface changes related to urbanization using Landsat 7 Enhanced Thematic Mapper Plus (ETM+) and Landsat 8 Operational Land Imager and Thermal Infrared Sensor (OLI-TIRS) data in Sebkha, Oran, Algeria. They focused on the multi-temporal relationship between surface temperature, land use and NDVI in the areas affected by salinity which was characterized by a specific geographical space and a fragile natural environment. Bindajam, et al. [20] employed Advanced Spaceborne Thermal Emission and Reflection Radiometer (ASTER) data for the retrieval of NDVI and LST in the cities of Abha-Khamis-Mushayet, South-Western province, Saudi Arabia. Also, Shah, et al. [19] used Landsat 8 OLI-TIR data to examine NDVI and LST over built-up and vegetative areas from 2013-2020 in Mehar taluka, Dadu, Sindh province, Pakistan. Furthermore, Guha, et al. [21] used premonsoon Landsat 5 Thematic Mapper (TM), Landsat 7, and Landsat 8 data for monitoring inter-relationship of LST with NDVI in Raipur City, India. Climate, vegetation types, land use, urbanization, etc. are factors influencing the correlation between the NDVI and the LST [27, 28]. Generally, the results from the above researches stated that NDVI and LST showed opposite trends.

This paper addressed 2 research questions: (1) Can satellite data be used for detection of gas flaring-related pollution on vegetation cover and its health in the Niger Delta? (2) What is the spatial and temporal variability in satellite detectable flare related pollution on vegetation cover and its health in the Niger Delta? Due to the above stated 2 research questions, the aim of this study is the generation of a Nigeria-focused technique for detection of gas flaring-related pollution on vegetation cover and its health using Landsat 7 and Landsat 8 data. Objectives for these 2 research questions are (1) Identification of significant gas flaring sites in the Niger Delta; (2) Determination of NDVI and LST for the selected sites; (3) Parameterization of flare-related change in NDVI as $(\delta NDVI_{450-60})_m$; (4) Detection of gas flaring-related pollution on vegetation cover and its health using NDVI data; (5) Evaluation of the relationship between the spatial gradient in NDVI and that of the LST around the flare sites in the Niger Delta.

2. Materials and Methods

2.1. Study Area

The study was conducted in Rivers State of the Niger Delta Region, Nigeria Figure 1. The selected 11 gas flaring sites used for the study are Eleme Petroleum Refinery Companies I and II, Bonny Liquefied Natural Gas (LNG) plant, Onne, Rukpokwu, Umurolu, Obigbo, Alua, Umudioga and Chokocho Flow Stations; and Sara oil well Figure 1C. All sites are located within Latitude 4° 40′ and 5° 01′ N and Longitude 6° 50′ and 7° 01′ E [1, 2] Figure 1C. In order to have adequate NDVI and LST data for appropriate analysis, (12 × 12) km area was studied around the flare stacks with Landsat 7 and Landsat 8 data.

2.2. Data used and Data Processing

2 acquired data used for this research are 21 Landsat 7 ETM+ scene dated from 2000 to 2013; and 4 Landsat 8 OLI-TIRS scene dated from 2018 to 2022 with <3 % cloud cover from the months of January to April, and November to December. They were acquired from the United States Geological Survey (USGS) website (https://earthexplorer.usgs.gov/). The selected data fall within the dry season in Nigeria. Hence, they are less cloudy. Landsat 7 ETM+ images consist of 8 spectral bands with a spatial resolution of 30 m for bands 1-5, and 7. The resolution for band 8 (Panchromatic) is 15 m. Landsat 8 OLI-TIRS images consist of 11 spectral bands with bands 1-7, and 9 having a spatial resolution of 30 m; and band 8 (Panchromatic) is 15 m. The spatial resolution for Landsat 7 band 6 (Thermal infrared), and Landsat 8 bands 10 and 11 (Thermal infrared) are 60 m and 100 m respectively but all are re-sampled to 30 m pixels [29]. MATLAB programming codes were used for data processing.
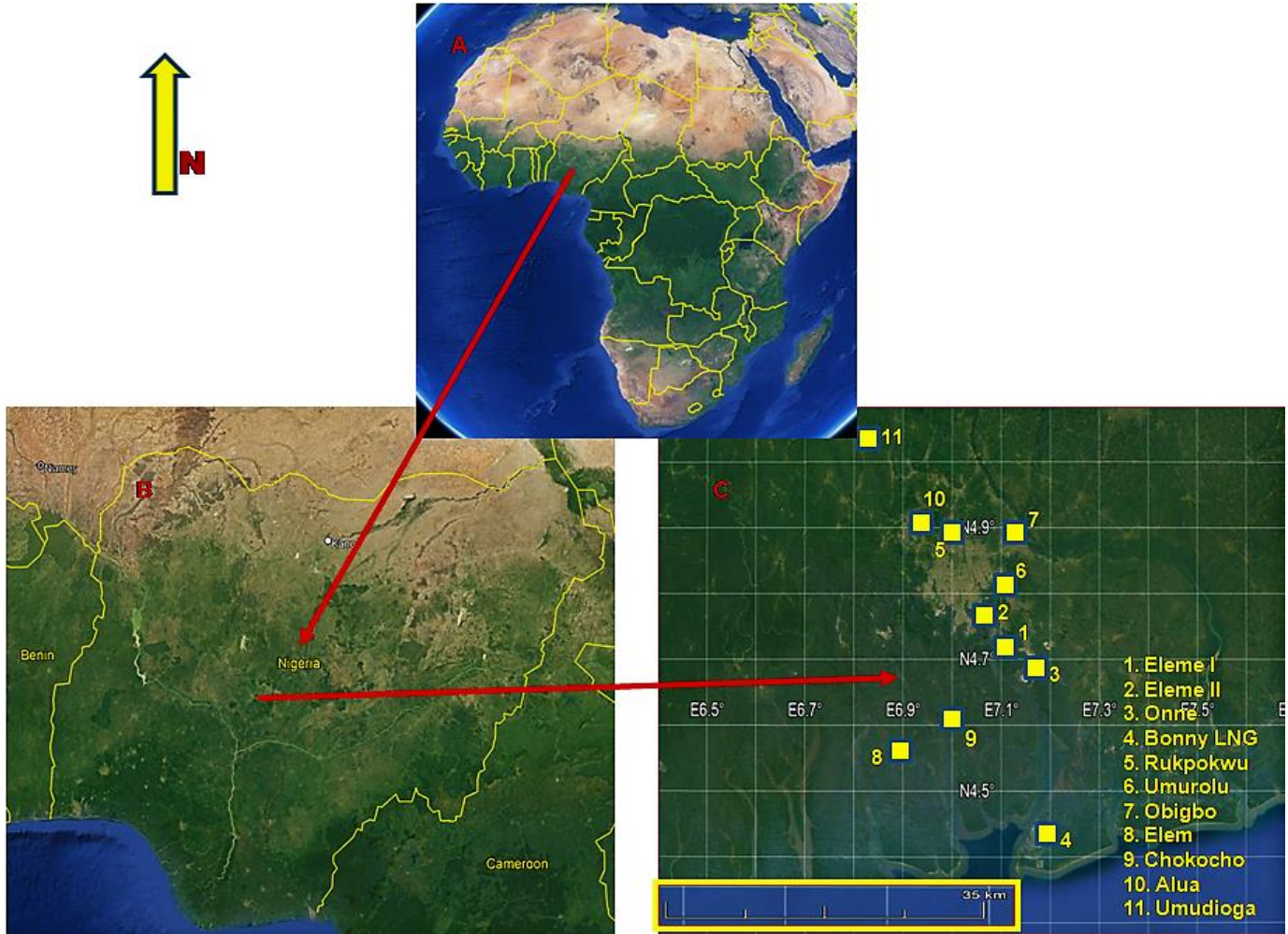

Figure 1. A) Map of Africa showing Nigeria [30]; B) Map of Nigeria [30]; C) Map of Rivers State with the 11 flaring sites examined [30].

2.3. Landsat Reflectance Retrieval

The computation of the spectral reflectance for Landsat 7 ETM+multispectral bands (1-4) and Landsat 8 OLI-TIRS multispectral bands (2-5) was carried out using Equation 1, Figure 2 which assumes Lambertian surface reflectance [31].

$$\rho_p = (\pi \times L_\lambda \times d^2) \div (ESUN_\lambda \times Cos\theta s) \tag{1}$$

Where: ρ_p = Spectral reflectance.
L = Surface leaving radiance/ unit solid angle.
πL = Upwelling radiance.
d = Earth-Sun distance/astronomical units.
$ESUN_\lambda$ = Mean solar exoatmospheric irradiances.
θs = Solar zenith incident angle/°.

2.4. Landsat Normalized Differential Vegetation Index (NDVI)Retrieval

NDVI is the most regularly used vegetation index is Huang, et al. [32]; Guha, et al. [33]. NDVI is an indicator of vegetation that is generally used in the study of vegetation and surface temperature relationship [34]. NDVI values are from −1 to +1 [31]. When NDVI value is −, it suggests surfaces like cloud, ocean, ice, water etc. NDVI values near zero indicate bare soil, sparse vegetation range from (0-0.01) to (0.1-0.5), and dense, green and healthy vegetation is 0.6 above.

The algorithm for NDVI is:

$$NDVI = (NIR - R) / (NIR + R) \, [18, 21] \tag{2}$$

Where:
NIR = Near Infra-Red reflectance, band 4 for Landsat 7, and band 5 for Landsat 8.
R = Red reflectance, band 3 for Landsat 7, and band 4 for Landsat 8.

For this research, atmospheric effects on Landsat data was corrected Figure 2 i.e. the cloud-masked reflectance was used for the computation of NDVI with Equation 2. Hence, NDVIs data from 2000 to 2022 was employed for detecting and assessing the potentially gas flaring-related pollution on vegetation cover and health.

Quantitative analysis of a change in vegetation cover and health was evaluated with the computed NDVIs at a given time using 2 analyses namely plot of NDVI versus distance from the flare in the North (N), East (E), South (S) and West (W) directions; and derivation of change in NDVI as (δNDVI$_{450-60}$)$_m$in the N, E, S and W directions.

2.5. Landsat Land Surface Temperature (LST) Retrieval

Retrieval of LST from Landsat data was carried out through radiative transfer equation in 3 stages [21, 35]. The 1st stage is the conversion of Digital Numbers (DN) of thermal bands to top of atmosphere (TOA) radiance using Equation 3 for Landsat 7 data; and Equation 4 for Landsat 8 images.

$$L_\lambda = ((LMAX_\lambda - LMIN_\lambda)/(QCALMAX - QCALMIN)) * (QCAL - QCALMIN) + LMIN_\lambda \quad (3)$$

Where:

L_λ= Spectral radiance (Wm^{-2}sr^{-1}μm^{-1}).

QCAL = Quantized calibrated pixel value in DN.

$LMIN_\lambda$= Spectral radiance scaled to QCALMIN (Wm^{-2}sr^{-1}μm^{-1}).

$LMAX_\lambda$= Spectral radiance scaled to QCALMAX (Wm^{-2}sr^{-1}μm^{-1}).

QCALMIN = Minimum quantized calibrated pixel value in DN = 1.

QCALMAX = Maximum quantized calibrated pixel value in DN = 255.

$$L_\lambda = M_L * QCA_L + A_L \quad (4)$$

Where M_L= Band multiplicative rescaling factor; A_L= Band additive rescaling factor. M_L and A_L are available in the metadata file of Landsat 8 data. L_λ and QCAL in (4) are the same as those in (3).

Conversion of TOA radiance of thermal band to surface-leaving radiance using atmospheric correction tool MODerate-Resolution Atmospheric Radiance and Transmittance (MODTRAN 4.1) for the removal of the effects of the atmosphere is the 2nd stage [36]. The surface-leaving radiance L_T is calculated using Equation 5 [37]:

$$L_T = (L_\lambda - L_\mu - \tau (1 - \varepsilon)L_d)/\tau\varepsilon \quad (5)$$

Where L_μ, L_d and τ= Upwelling radiance, downwelling radiance, and atmospheric transmission respectively. They are atmospheric correction parameters for Landsat thermal band. ε = Emissivity of land covers (LC) type. For this study, ε was calculated based on 4 LC (Vegetation, built area, soil and water) types of each site.

For the 3rd stage, the surface-leaving radiance is converted to LST using Landsat estimate of the Planck curve Equation 6 [38] Figure 2:

$$LST = \frac{K_2}{\ln((K_1/L_\lambda) + 1)} \quad (6)$$

Where,

LST = Land Surface Temperature in Kelvin (K); K_1 and K_2 = Thermal band calibration constants Table 1. LSTs for vegetation, built area, soil and water were retrieved but only LSTs for vegetation was adopted for the analysis.

Table 1. Calibration constants K_1 and K_2 for Landsat 7 and Landsat 8 data.

Calibration constants	Landsat 7 ETM+	Landsat 8 band 10	Landsat 8 band 11
K_1 (Wm^{-2}sr^{-1}μm^{-1})	666.09	774.89	480.89
K_2 (K)	1282.71	1321.08	1201.14

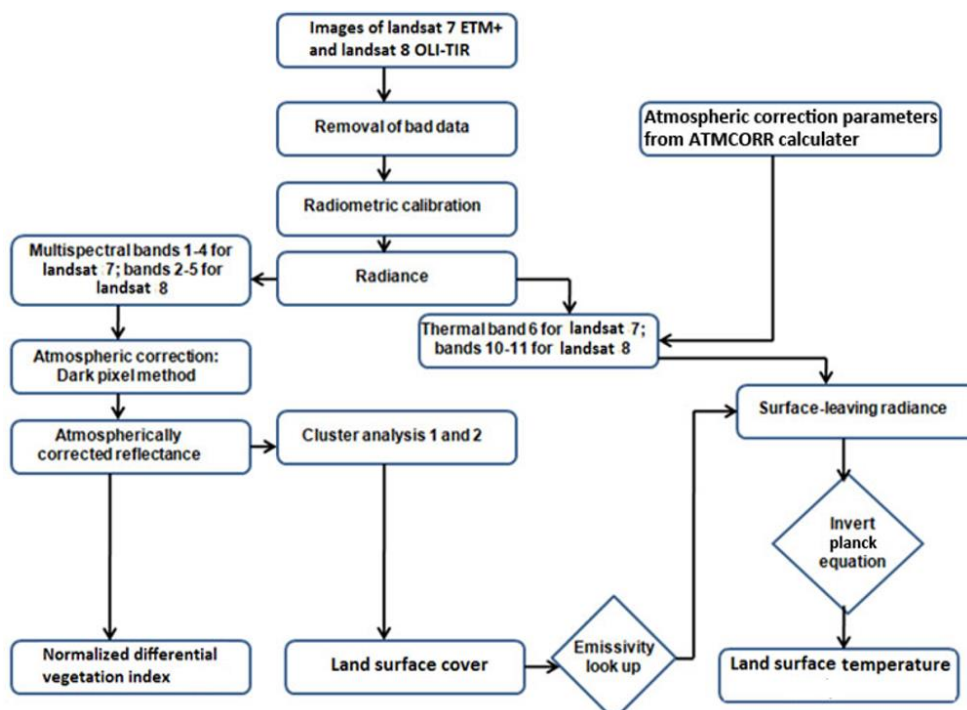**Source:** USGS [29].

Figure 2. Flow chart for the methodology adopted.

2.6. NDVI Versus Distance

At 60 m and 450 m distance from the flare stack, values of NDVIs were recorded Figure 3 in the N, E, S and W directions. Also, the range of NDVIs values was computed.

2.7. Change in NDVI $(\delta NDVI_{450-60})_m$ and LST $(\delta LST_{60-450})_m$

Change in NDVI (δNDVI) is the difference in the values of NDVI recorded at 450 m distance from the flare stack and that of the values of NDVIs obtained at 60 m from the stack.

i.e. $NDVI_{450} - NDVI_{60m} = (\delta NDVI_{450-60})_m$.

Figure 3 is the schematic diagram for $(\delta NDVI_{450-60})_m$. $(\delta NDVI_{450-60})_m$ was computed for N, E, S and W directions, hence, $(\delta NDVI_{450-60})_m N$, $(\delta NDVI_{450-60})_m E$, $(\delta NDVI_{450-60})_m S$ and $(\delta NDVI_{450-60})_m W$ were obtained. This is to help in assessing the vegetation cover and its health in the 4 directions.
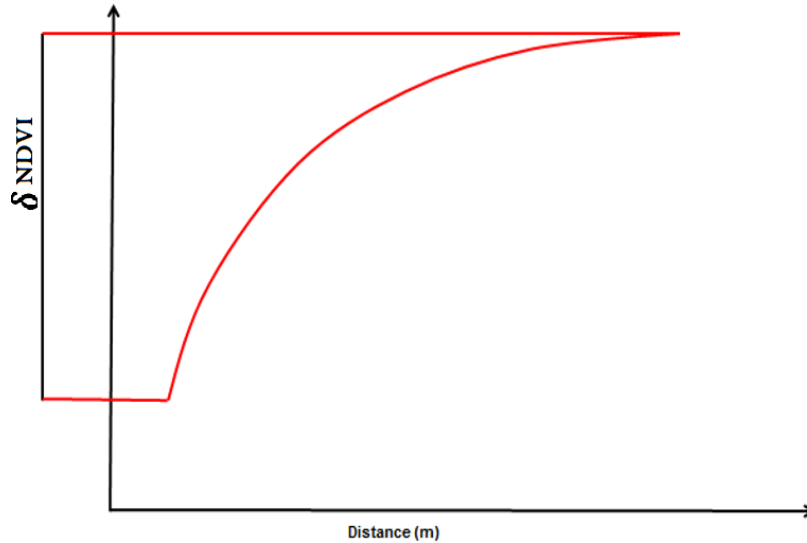

Figure 3. Schematic diagram for change in NDVI $(\delta NDVI_{450-60})_m$.

For change in LST $(\delta LST_{60-450})_m$, it is the difference in the values of LSTs at the 60 m from the flare stack and that of values of LST at 450 m from the flare stack [1, 5].

i.e. $LST_{60} - LST_{450m} = (\delta LST_{60-450})_m$. This means that the distance adopted for the computation of $(\delta NDVI_{450-60})_m$ is the reverse of the distance chosen for the computation of $(\delta LST_{60-450})_m$.

2.8. Linear Regression Analysis

NDVI-LST relationship has been investigated by researchers using linear regression analysis. Such researchers include [18, 19, 39]. In addition, non-linear regression was employed by Cleland, et al. [40]; Sparks and Tryjanowski [41]; Dose and Menzel [42] for studying the effects of global change on plant phenology. This study adopted linear regression analysis because non-linear regression gives no better results when tested. Hence, $(\delta NDVI_{450-60})_m$ and $(\delta LST_{60-450})_m$ relationship in the N, E, S and W were examined when no data is zero in order to eliminate the effects of uncertainties. When $(\delta NDVI_{450-60})_m = 0$, it means that the values of NDVI at both 60 m and 450 m from the stack are equal, suggesting an uncertain condition. Similarly, when $(\delta LST_{60-450})_m = 0$, it means that the values of LST at 60 m and 450 m from the stack are equal; suggesting the availability of other heat sources at 450 m or no burning on the stack at the time of satellite overpass. Table 15 presents r-values and p-values results obtained from the analysis. N = total number of each $(\delta NDVI_{450-60})_m$'s and $(\delta LST_{60-450})_m$'s used, r-values show the type of correlation that existed between them, and p-values show whether the results obtained are statistically significant or insignificant with apriori $\alpha = 0.01$.

3. Results and Discussion

3.1. NDVI Versus Distance

Tables 2-13 present the values of NDVI recorded at 60 m and 450 m from the stack for the 11 sites studied for the year 2000, 2011 and 2022 respectively.

Table 2. NDVI retrieved at 60 m and 450 m from the stack (North direction) (2000).

Flaring site	NDVI at 60 m	NDVI at 450 m	$(\delta NDVI_{450-60})_m$
Eleme refinery I	0.35	0.74	0.39
Eleme refinery II	0.18	0.52	0.34
Onne	0.22	0.75	0.53
Umurolu	0.22	0.48	0.26
Bonny LNG	0.20	0.50	0.30
Alua	0.18	0.76	0.58
Rukpokwu	0.20	0.68	0.48
Obigbo	0.19	0.53	0.34
Chokocho	0.18	0.56	0.38
Umudioga	0.21	0.71	0.50
Sara	0.18	0.62	0.44

Table 3. NDVI retrieved at 60 m and 450 m from the stack (East direction) (2000).

Flaring site	NDVI at 60 m	NDVI at 450 m	$(\delta NDVI_{450-60})_m$
Eleme refinery I	0.41	0.78	0.37
Eleme refinery II	0.48	0.63	0.15
Onne	0.27	0.77	0.50
Umurolu	0.36	0.54	0.18
Bonny LNG	0.41	0.58	0.17
Alua	0.36	0.74	0.38
Rukpokwu	0.49	0.75	0.26
Obigbo	0.35	0.64	0.29
Chokocho	0.32	0.59	0.27
Umudioga	0.40	0.75	0.35
Sara	0.34	0.70	0.36

Table 4. NDVI retrieved at 60 m and 450 m from the stack (South direction) (2000).

Flaring site	NDVI at 60 m	NDVI at 450 m	$(\delta NDVI_{450-60})_m$
Eleme refinery I	0.47	0.82	0.35
Eleme refinery II	0.30	0.60	0.30
Onne	0.34	0.71	0.37
Umurolu	0.35	0.56	0.21
Bonny LNG	0.32	0.58	0.26
Alua	0.31	0.79	0.48
Rukpokwu	0.36	0.74	0.38
Obigbo	0.35	0.59	0.24
Chokocho	0.25	0.64	0.39
Umudioga	0.26	0.77	0.51
Sara	0.21	0.68	0.47

Table 5. NDVI retrieved at 60 m and 450 m from the stack (West direction) (2000).

Flaring site	NDVI at 60 m	NDVI at 450 m	$(\delta NDVI_{450-60})_m$
Eleme refinery I	0.38	0.83	0.45
Eleme refinery II	0.21	0.62	0.41
Onne	0.25	0.84	0.59
Umurolu	0.27	0.60	0.33
Bonny LNG	0.38	0.58	0.20
Alua	0.36	0.84	0.48
Rukpokwu	0.37	0.74	0.37
Obigbo	0.30	0.61	0.31
Chokocho	0.25	0.69	0.44
Umudioga	0.24	0.77	0.53
Sara	0.44	0.73	0.29

Table 6. NDVI retrieved at 60 m and 450 m from the stack (North direction) (2011).

Flaring site	NDVI at 60 m	NDVI at 450 m	$(\delta NDVI_{450-60})_m$
Eleme refinery I	0.25	0.68	0.43
Eleme refinery II	0.10	0.59	0.49
Onne	0.17	0.71	0.54
Umurolu	0.18	0.50	0.32
Bonny LNG	0.16	0.48	0.32
Alua	0.12	0.79	0.67
Rukpokwu	0.13	0.62	0.49
Obigbo	0.14	0.59	0.45
Chokocho	0.11	0.54	0.43
Umudioga	0.16	0.73	0.57
Sara	0.12	0.55	0.43

Table 7. NDVI retrieved at 60 m and 450 m from the stack (East direction) (2011).

Flaring site	NDVI at 60 m	NDVI at 450 m	$(\delta NDVI_{450-60})_m$
Eleme refinery I	0.21	0.66	0.36
Eleme refinery II	0.18	0.57	0.39
Onne	0.22	0.71	0.49
Umurolu	0.23	0.52	0.29
Bonny LNG	0.21	0.45	0.24
Alua	0.21	0.75	0.58
Rukpokwu	0.20	0.60	0.40
Obigbo	0.17	0.57	0.38
Chokocho	0.19	0.51	0.33
Umudioga	0.23	0.71	0.50
Sara	0.15	0.53	0.36

Table 8. NDVI retrieved at 60 m and 450 m from the stack (South direction) (2011).

Flaring site	NDVI at 60 m	NDVI at 450 m	$(\delta NDVI_{450-60})_m$
Eleme refinery I	0.32	0.61	0.29
Eleme refinery II	0.20	0.50	0.30
Onne	0.23	0.64	0.41
Umurolu	0.23	0.45	0.22
Bonny LNG	0.16	0.43	0.27
Alua	0.12	0.68	0.56
Rukpokwu	0.13	0.55	0.42
Obigbo	0.14	0.69	0.55
Chokocho	0.11	0.55	0.44
Umudioga	0.16	0.69	0.53
Sara	0.12	0.58	0.46

Table 9. NDVI retrieved at 60 m and 450 m from the stack (West direction) (2011).

Flaring site	NDVI at 60 m	NDVI at 450 m	$(\delta NDVI_{450-60})_m$
Eleme refinery I	0.25	0.73	0.48
Eleme refinery II	0.14	0.61	0.47
Onne	0.19	0.68	0.49
Umurolu	0.20	0.51	0.31
Bonny LNG	0.18	0.50	0.32
Alua	0.14	0.68	0.54
Rukpokwu	0.16	0.58	0.42
Obigbo	0.20	0.57	0.37
Chokocho	0.15	0.53	0.38
Umudioga	0.17	0.69	0.52
Sara	0.16	0.52	0.36

Table 10. NDVI retrieved at 60 m and 450 m from the stack (North direction) (2022).

Flaring site	NDVI at 60 m	NDVI at 450 m	$(\delta NDVI_{450-60})_m$
Eleme refinery I	0.12	0.70	0.58
Eleme refinery II	0.12	0.60	0.48
Onne	0.12	0.71	0.59
Umurolu	0.13	0.52	0.39
Bonny LNG	0.14	0.55	0.41
Alua	0.11	0.68	0.57
Rukpokwu	0.13	0.71	0.58
Obigbo	0.12	0.58	0.46
Chokocho	0.13	0.57	0.44
Umudioga	0.10	0.65	0.55
Sara	0.11	0.58	0.47

Table 11. NDVI retrieved at 60 m and 450 m from the stack (East direction) (2022).

Flaring site	NDVI at 60 m	NDVI at 450 m	$(\delta NDVI_{450-60})_m$
Eleme refinery I	0.12	0.71	0.59
Eleme refinery II	0.11	0.59	0.48
Onne	0.12	0.68	0.56
Umurolu	0.11	0.53	0.42
Bonny LNG	0.10	0.57	0.47
Alua	0.13	0.64	0.51
Rukpokwu	0.12	0.70	0.58
Obigbo	0.11	0.60	0.49
Chokocho	0.10	0.53	0.43
Umudioga	0.12	0.61	0.49
Sara	0.10	0.51	0.41

Table 12. NDVI retrieved at 60 m and 450 m from the stack (South direction) (2022).

Flaring site	NDVI at 60 m	NDVI at 450 m	$(\delta NDVI_{450-60})_m$
Eleme refinery I	0.10	0.55	0.45
Eleme refinery II	0.13	0.64	0.51
Onne	0.08	0.68	0.60
Umurolu	0.11	0.58	0.47
Bonny LNG	0.13	0.61	0.48
Alua	0.11	0.63	0.52
Rukpokwu	0.12	0.61	0.49
Obigbo	0.09	0.49	0.40
Chokocho	0.08	0.50	0.42
Umudioga	0.08	0.64	0.56
Sara	0.10	0.60	0.50

Table 13. NDVI retrieved at 60 m and 450 m from the stack (West direction) (2022).

Flaring site	NDVI at 60 m	NDVI at 450 m	$(\delta NDVI_{450-60})_m$
Eleme refinery I	0.11	0.59	0.48
Eleme refinery II	0.14	0.62	0.48
Onne	0.13	0.67	0.54
Umurolu	0.09	0.60	0.51
Bonny LNG	0.10	0.54	0.44
Alua	0.12	0.63	0.51
Rukpokwu	0.11	0.65	0.54
Obigbo	0.09	0.54	0.45
Chokocho	0.10	0.57	0.47
Umudioga	0.12	0.68	0.56
Sara	0.11	0.61	0.50

Generally, Tables 2-13 show that the values of NDVI at 60 m from the flare stack is much lower. For example for the year 2022, NDVIs recorded are the lowest (0.08-0.14). This suggests little or no vegetation cover, bear soil etc within the area. However, at 450 m from the stack, the values of NDVI are higher (0.43-0.84) which suggests that the vegetation cover is not sparse but green and healthy. Therefore, the results showed that the vegetation cover and its health around the flare stack have been negatively affected by the flare leading to the sparse or no vegetation cover [21, 43]. NDVI values at 60 m from the flare reduce even to almost zero while LST values are higher. This is supported by previous researches [18, 20, 22-26]. This suggest that the vegetation cover is unhealthy and polluted, some have died, many are dying, while others have been reduced to almost bear soil as a result of the continuous effects of pollution from the flare. However, the NDVI values at 450 m did not follow a uniform trend, their values changes. This may be resulted from some external activities apart from gas flaring within the area.

3.2. Change in NDVI $(\delta NDVI_{450-60})_m$

Figures 4-6 are the plots for the $(\delta NDVI_{450-60})_m N$ against $(\delta NDVI_{450-60})_m E$, $(\delta NDVI_{450-60})_m N$ against $(\delta NDVI_{450-60})_m S$ and $(\delta NDVI_{450-60})_m N$ against $(\delta NDVI_{450-60})_m W$ for the 11 facilities studied. The number (N) of $(\delta NDVI_{450-60})_m$ used for each of the plot is 348. Data for each facility is identified using the colour of the stack height. For exampleEleme Refinery I has the stack height of 50 m and that of Eleme Refinery II is 65 m. Hence, all deep red and brown points in these figures are from these 2 refineries.
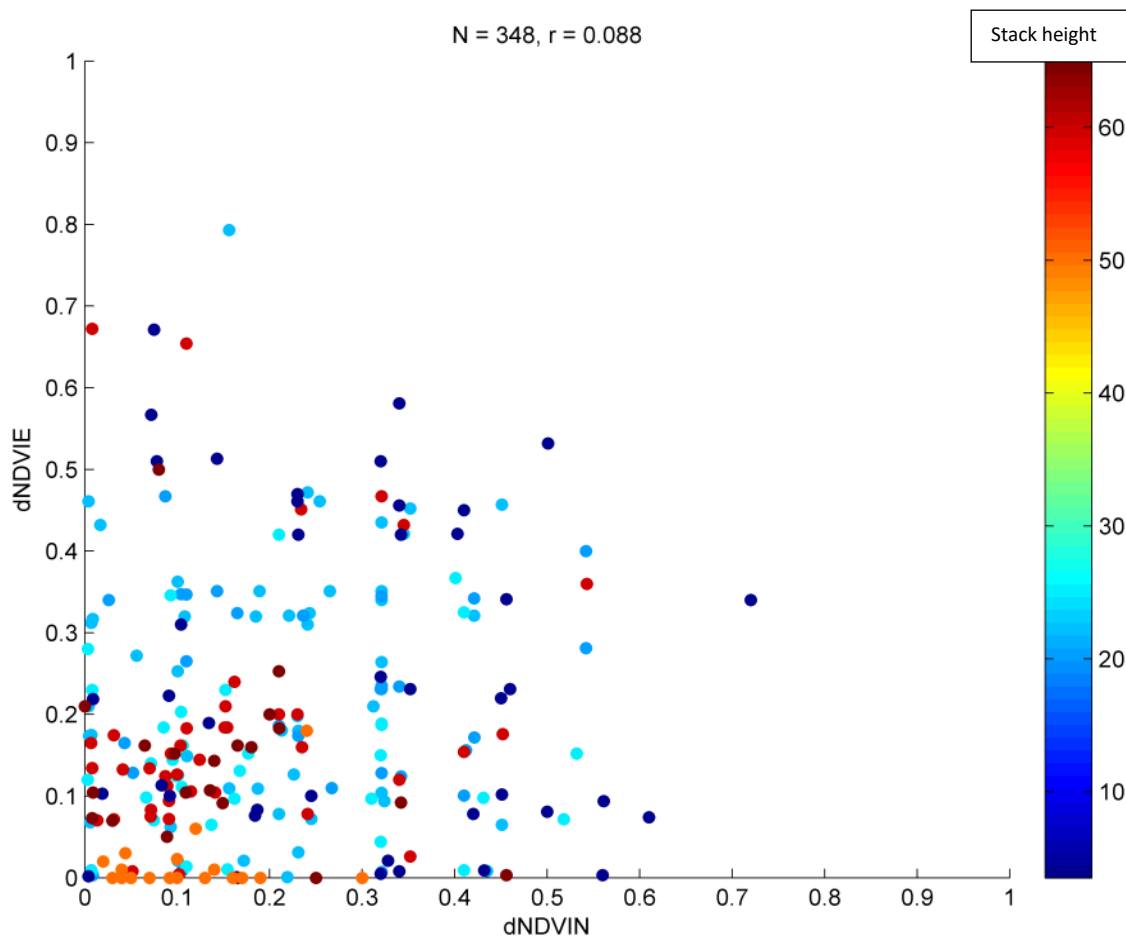

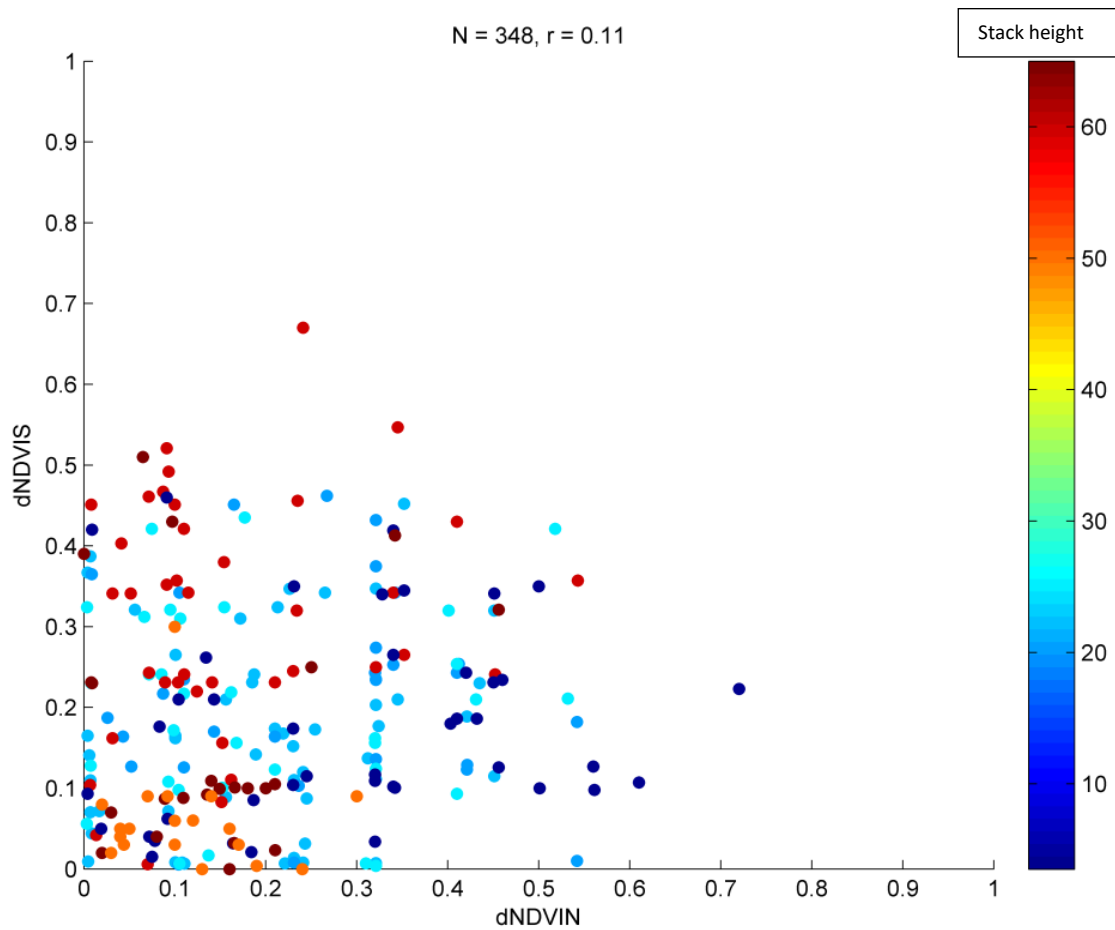**Figure 4.** $(\delta NDVI_{450-60})_m N$ against $(\delta NDVI_{450-60})_m E$.

Figure 5. $(\delta NDVI_{450-60})_m N$ against $(\delta NDVI_{450-60})_m S$.

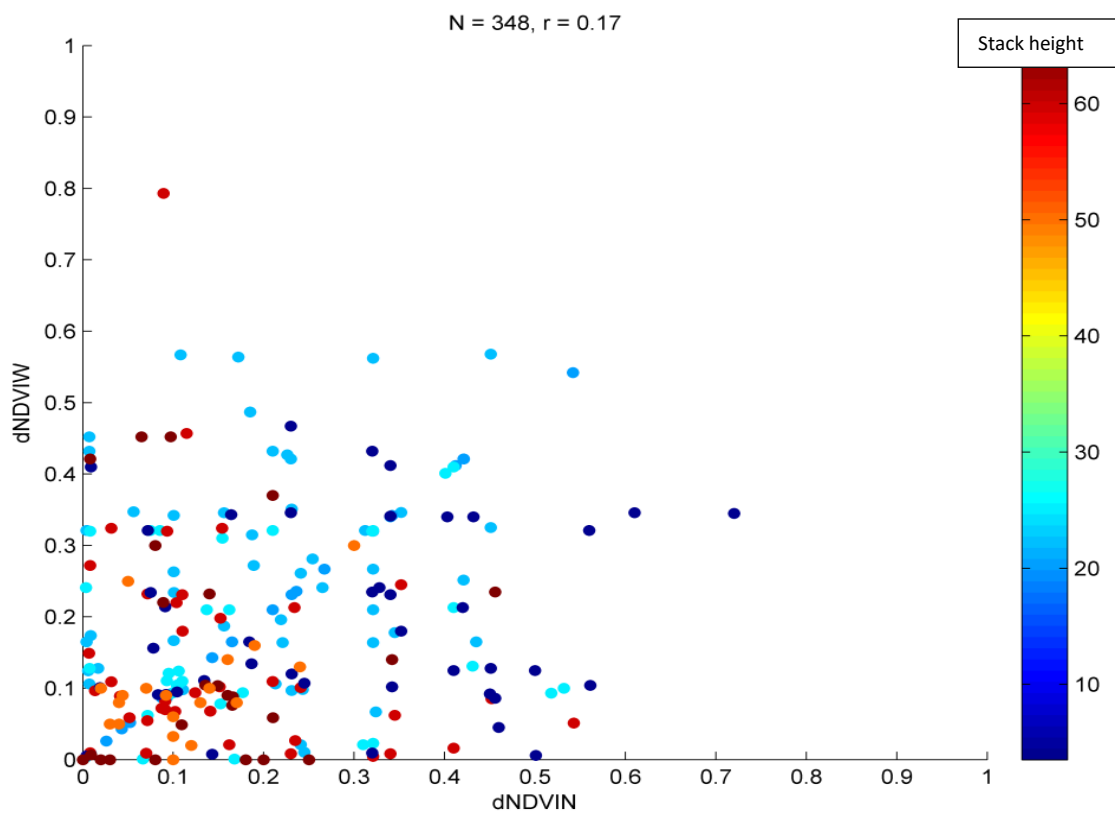**Figure 6.** $(\delta NDVI_{450-60})_m N$ against $(\delta NDVI_{450-60})_m W$.

Table 14 presents the results obtained when $(\delta NDVI_{450-60})_m N$ versus $(\delta NDVI_{450-60})_m E$, $(\delta NDVI_{450-60})_m N$ versus $(\delta NDVI_{450-60})_m S$ and $(\delta NDVI_{450-60})_m N$ versus $(\delta NDVI_{450-60})_m W$ relationships are considered. All results show positive correlation, but only $(\delta NDVI_{450-60})_m N$ versus $(\delta NDVI_{450-60})_m W$ give statistically significant result at 99 % confidence level (p-values = 0.0016) whilst the other 2 are not statistically significant.

Table 14. Results for $(\delta NDVI_{450-60})_m$ against North, East, South and West directions with $\boldsymbol{\alpha}$ = 0.01.

Relationship	R-value	P-value	Type of correlation
$(\delta NDVI_{450-60})_m N$ v $(\delta NDVI_{450-60})_m E$	0.08	0.11	Positive (+)
$(\delta NDVI_{450-60})_m N$ v $(\delta NDVI_{450-60})_m S$	0.10	0.07	Positive (+)
$(\delta NDVI_{450-60})_m N$ v $(\delta NDVI_{450-60})_m W$	0.17	0.00	Positive (+)

3.3. Linear Regression Analysis for $(\delta NDVI_{450-60})_m$ against $(\delta LST_{60-450})_m$

Table 15 presented the results of the analysis of $(\delta NDVI_{450-60})_m$ against $(\delta LST_{60-450})_m$ in the N, E, S, and W directions. The total number (N) of $(\delta NDVI_{450-60})_m$ against $(\delta LST_{60-450})_m$ for each facility used for the analysis in the 4 directions, the r-values and p-values obtained in the 4 directions are presented.

Table 15. $(\delta NDVI_{450-60})_m$ against $(\delta LST_{60-450})_m$ (when both > 0) with $\alpha = 0.01$.

Facility	Number (N), r-value, p-value (North direction)	Number (N), r-value, p-value (East direction)	Number (N), r-value, p-value (South direction)	Number (N), r-value, p-value (West direction)
1: Eleme I	15.0	14.0	15.0	13.0
	0.56	-0.22	-0.20	-0.06
	0.03	0.44	0.45	0.81
2: Eleme II	17.0	19.0	17.0	17.0
	0.16	-0.02	0.32	0.60
	0.53	0.87	0.19	0.01
3: Onne	23.0	27.0	27.0	31.0
	-0.13	0.13	0.14	-0.31
	0.44	0.45	0.42	0.07
4: Umurolu	22.0	29.0	28.0	27.0
	-0.06	-0.14	-0.24	0.03
	0.79	0.53	0.23	0.90
5: Bonny	15.0	24.0	20.0	23.0
	0.17	0.14	-0.15	0.22
	0.62	0.65	0.62	0.21
6: Alua	20.0	17.0	20.0	18.0
	0.23	-0.18	0.02	0.15
	0.32	0.62	0.98	0.46
7: Rukpokwu	30.0	26.0	31.0	30.0
	-0.17	-0.27	0.42	-0.01
	0.32	0.17	0.03	0.98
8: Obigbo	24.0	18.0	20.0	18.0
	-0.08	0.16	-0.20	-0.37
	0.72	0.46	0.36	0.11
9: Chokocho	21.0	20.0	22.0	20.0
	-0.20	0.27	0.16	0.29
	0.38	0.25	0.42	0.22
10: Umudioga	12.0	14.0	16.0	18.0
	-0.04	-0.14	0.42	-0.03
	0.86	0.33	0.06	0.95
11: Sara	15.0	25.0	31.0	29.0
	-0.09	0.17	-0.04	-0.09
	0.72	0.35	0.83	0.68

In Table 15, Eleme Refineries I and II, Bonny LNG and Alua Flow Station have positive (+) correlation and statistically insignificant results in the N direction. Onne, Umurolu, Rukpokwu, Obigbo, Chokocho, Umudioga Flow Stations, and Sara oil well show negative (−) r-values and insignificant p-values in the N direction. In the E direction, Eleme Refineries I and II; Umurolu, Alua and Umudioga Flow Stations also have − r-values and insignificant p-values; and Bonny LNG; Onne, Obigbo, Chokocho Flow Stations; and Sara oil well have a + correlation and insignificant results. In the S direction Eleme Refinery, I; Bonny LNG; and Umurolu and Obigbo Flow Stations; and Sara oil well give − r-values and insignificant p-values. Furthermore, Eleme Refinery II; Onne, Alua, Rukpokwu, Chokocho and Umudioga Flow Stations have + r-values and insignificant p-values. Finally, in the W direction, Eleme Refinery I; Onne, Rukpokwu, Obigbo, Umudioga Flow Stations; and Sara oil well show − r-values and insignificant p-values. Eleme Refinery II; Bonny LNG; Umurolu, Alua and Chokocho Flow Stations show + r-values and insignificant p-values.

Results in Table 16 are obtained from the linear regression analysis for $(\delta NDVI_{450-60})_m$ and $(\delta LST_{60-450})_m$ when North, East, South, and West directions were evaluated with $\alpha = 0.01$ for all the 11 facilities processed together.

Table 16. Results obtained for $\delta NDVI$ against δLST with $\alpha = 0.01$.

Relationship	Number	r-values	p-values	Type of correlation
$(\delta NDVI_{450-60})_m N$ v $(\delta LST_{60-450})_m N$	214	0.00	0.97	Positive (+)
$(\delta NDVI_{450-60})_m E$ v $(\delta LST_{60-450})_m E$	233	0.09	0.20	Positive (+)
$(\delta NDVI_{450-60})_m S$ v $(\delta LST_{60-450})_m S$	249	0.03	0.20	Positive (+)
$(\delta NDVI_{450-60})_m W$ v $(\delta LST_{60-450})_m W$	244	0.10	0.11	Positive (+)

Figures 7-10 show the plots of the $(\delta NDVI_{450-60})_m N$ versus $(\delta LST_{60-450})_m N$, $(\delta NDVI_{450-60})_m E$ versus $(\delta LST_{60-450})_m E$, $(\delta NDVI_{450-60})_m S$ versus $(\delta LST_{60-450})_m S$, and $(\delta NDVI_{450-60})_m W$ versus $(\delta LST_{60-450})_m W$. The scale bar is an arbitrary chosen number for the identification of individual facility. For example, 1 represents Eleme Refinery I, 5 for Bonny LNG plant and 11 is for Sara Flow Station.
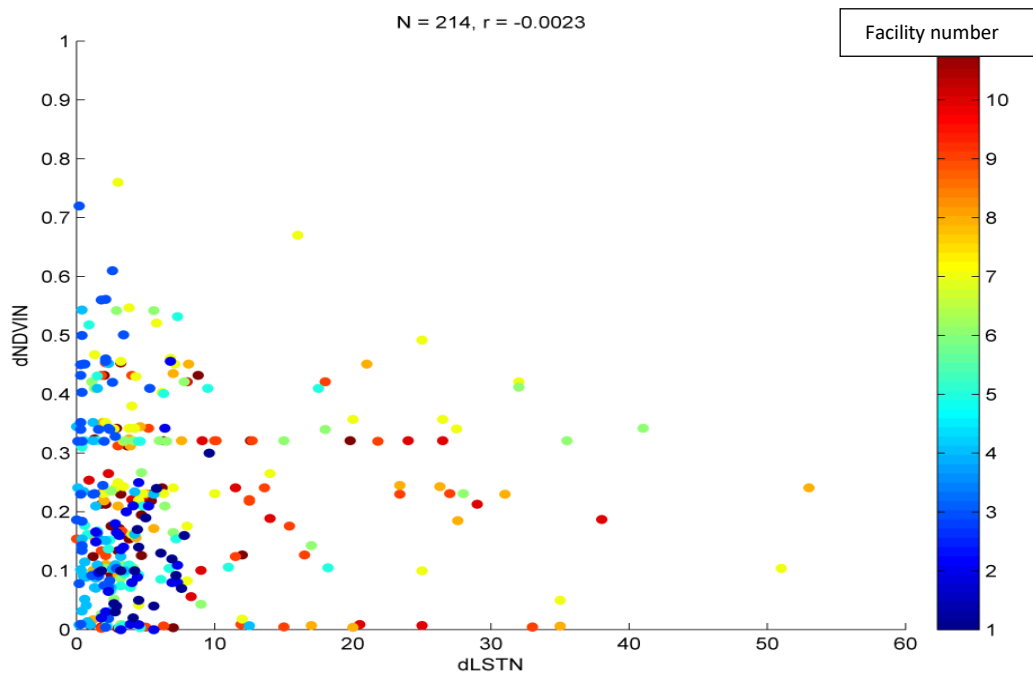
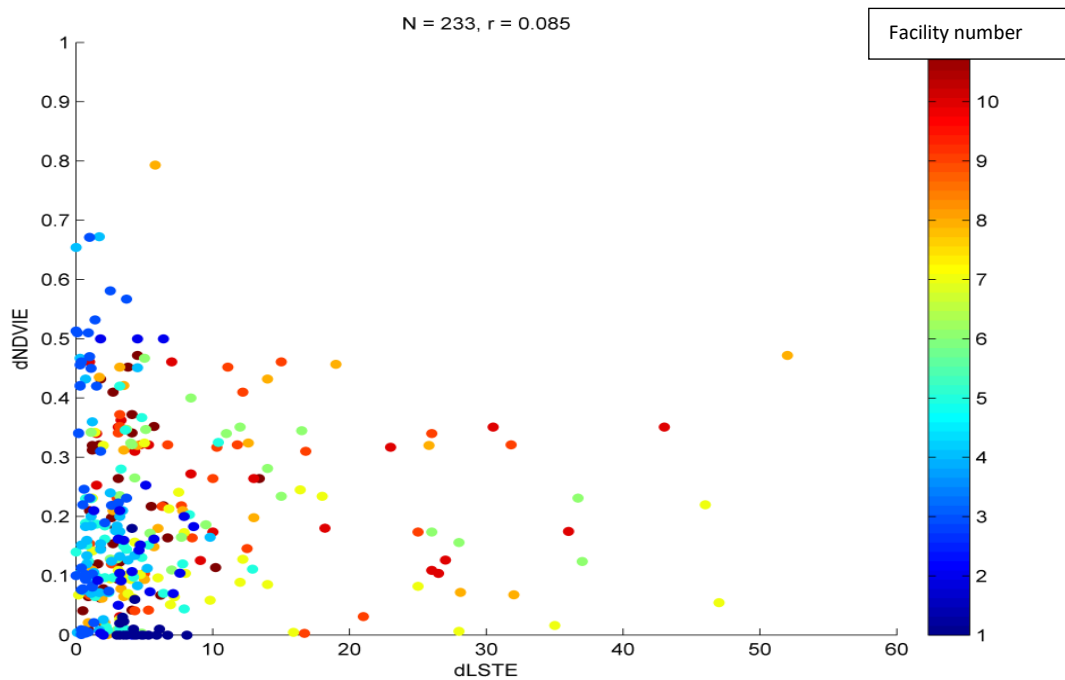**Figure 7.** $(\delta \text{NDVI}_{450-60})_m \text{N}$ against $(\delta \text{LST}_{60-450})_m \text{N}$.

Figure 8. $(\delta \text{NDVI}_{450-60})_m \text{E}$ against $(\delta \text{LST}_{60-450})_m \text{E}$.
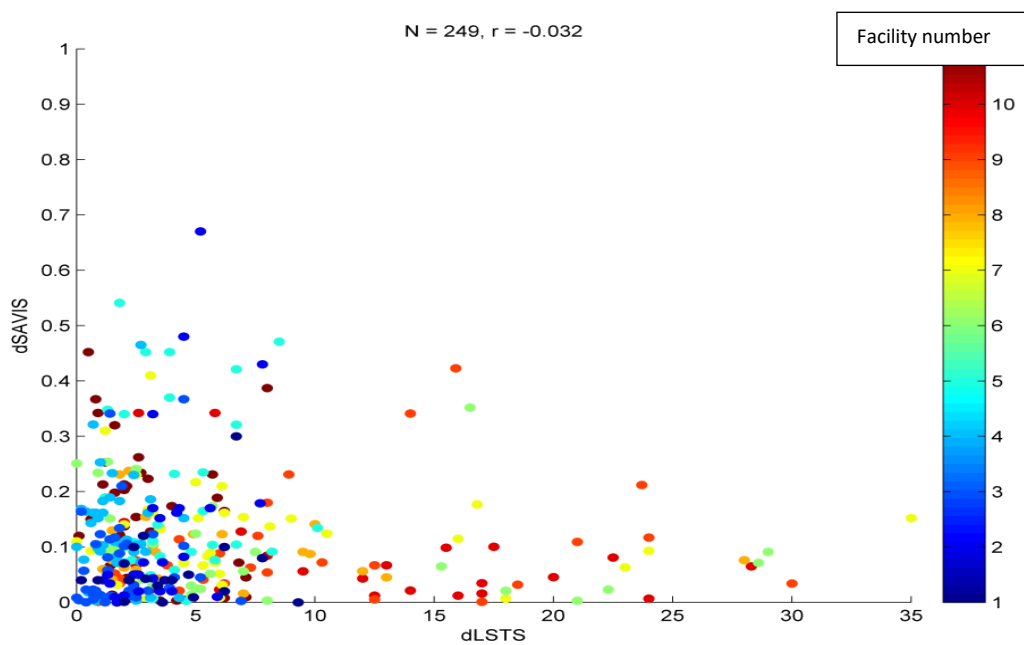
Figure 9. $(\delta \text{NDVI}_{450-60})_m \text{S}$ against $(\delta \text{LST}_{60-450})_m \text{S}$.
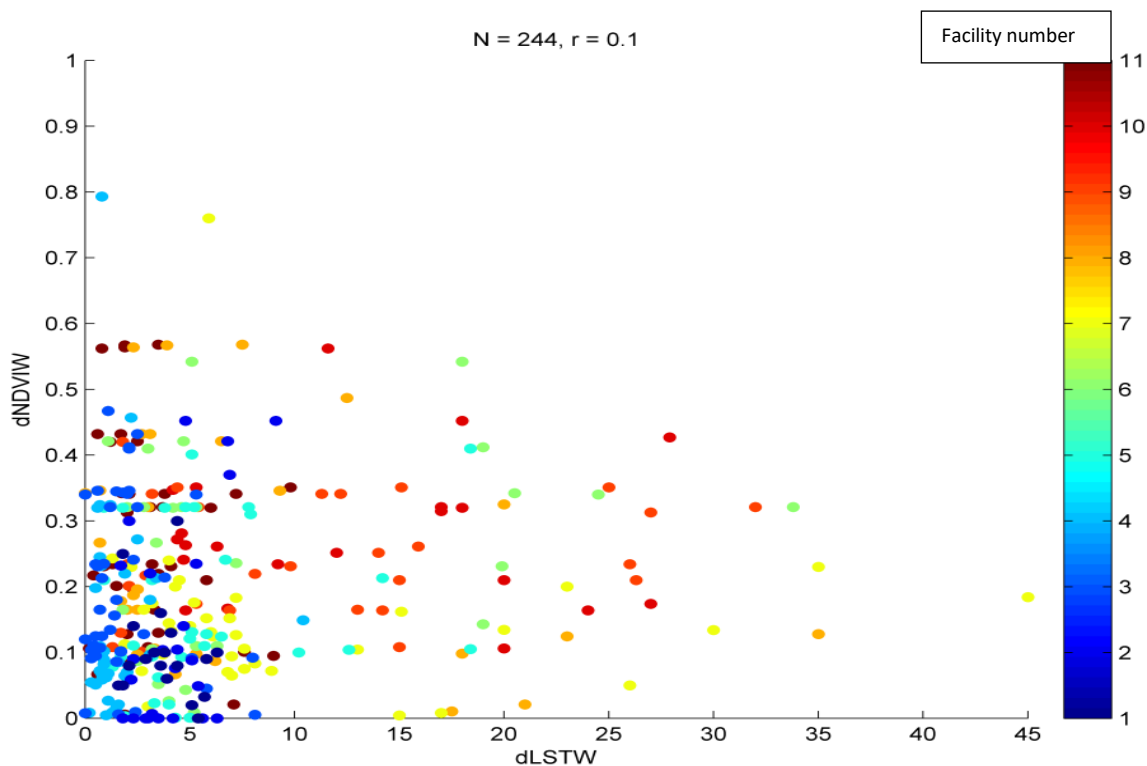
Figure 10. $(\delta\text{NDVI}_{450\text{-}60})_m\text{W}$ against $(\delta\text{LST}_{60\text{-}450})_m\text{W}$.

4. Conclusion

Only the correlation coefficient for Eleme I in the N direction (0.5558) and Eleme II in the W direction (0.6002) show that there is linear interdependence of the 2 variables, $(\delta\text{NDVI}_{450\text{-}60})_m$ and $(\delta\text{LST}_{60\text{-}450})_m$ (Table 15). However, the rest 9 facilities show non-linear interdependence of the 2 variables in the N, E, S and W. Therefore, due to lack of significant correlations no conclusions can be drawn about the effect of the prevailing wind direction (South) in the Niger Delta on any of the relationship between $(\delta\text{NDVI}_{450\text{-}60})_m$ and $(\delta\text{LST}_{60\text{-}450})_m$. Also, the results in Table 16 for the 4 relationships $(\delta\text{NDVI}_{450\text{-}60})_m\text{N}$ against $(\delta\text{LST}_{60\text{-}450})_m\text{N}$, $(\delta\text{NDVI}_{450\text{-}60})_m\text{E}$ against $(\delta\text{LST}_{60\text{-}450})_m\text{E}$, $(\delta\text{NDVI}_{450\text{-}60})_m\text{S}$ against $(\delta\text{LST}_{60\text{-}450})_m\text{S}$, and $(\delta\text{NDVI}_{450\text{-}60})_m\text{W}$ against $(\delta\text{LST}_{60\text{-}450})_m\text{W}$ considered shows positive correlation but statistically insignificant results. Based on the results obtained for this research, it can be concluded that gas flaring related pollution can be detected on vegetation cover and its health using Landsat 7 and Landsat 8 remotely sensed data in the Niger Delta.

Some challenges are encountered in this research, for example, the available Landsat data covers only dry season in Nigeria, hence a further research is required to examine and compare the NDVI and LST results for the rainy period data too. The recommendations made regarding this research are: (1) Nigerian Government should make sure the exorbitant penalty fee is paid by defaulters' oil and gas companies who refuse to adhere to flaring law and regulations; (2) All Nigerian should not lose the focus for the quest of having zero gas flaring in Nigeria.

References

[1]   B. Morakinyo, S. Lavender, and V. Abbott, "Investigation of potential prevailing wind impact on land surface temperature at gas flaring sites in the Niger Delta, Nigeria," *International Journal of Environment and Geoinformatics*, vol. 9, no. 1, pp. 179-190, 2022. https://doi.org/10.30897/ijegeo.968687

[2]   B. Morakinyo, S. Lavender, and V. Abbott, "The methodology and results from ground validation of satellite observations at gas Flaring Sites in Nigeria," *International Journal of Environment and Geoinformatics*, vol. 8, no. 3, pp. 290-300, 2021. https://doi.org/10.30897/ijegeo.749664

[3]   B. Morakinyo, S. Lavender, and V. Abbott, "Retrieval of land surface temperature from Earth observation satellites for gas flaring sites in the Niger Delta, Nigeria," *International Journal of Environmental Monitoring and Analysis*, vol. 8, no. 3, pp. 59-74, 2020. https://doi.org/10.11648/j.ijema.20200803.13

[4]   B. Morakinyo, S. Lavender, J. Schwarz, and V. Abbott, "Mapping of land cover and estimation of their emissivity values for gas flaring sites in the Niger Delta," *British Journal of Environmental Sciences*, vol. 7, no. 2, pp. 31-58, 2019.

[5]   B. O. Morakinyo, "Flaring and pollution detection in the niger delta using remote sensing," Ph.D Thesis, University of Plymouth, Plymouth, United Kingdom, 2015.

[6]   G. C. C. Ndinwa, S. A. Akpafun, and C. O. Chukumah, "Perceived environmental and health impacts of gas flaring on residents in Kwale Communities, Southern Nigeria," *Asian Journal of Energy Transformation and Conservation*, vol. 4, no. 1, pp. 1-21, 2020.

[7]   A. Caseiro, B. Gehrke, G. Rücker, D. Leimbach, and J. W. Kaiser, "Gas flaring activity and black carbon emissions in 2017 derived from the Sentinel-3A Sea and Land Surface Temperature Radiometer," *Earth System Science Data*, vol. 12, no. 3, pp. 2137-2155, 2020. https://doi.org/10.5194/essd-12-2137-2020

[8]   A. Zoeir, A. Tabatabaei Nejad, and E. Khodapanah, "Impact of H2S content and excess air on pollutant emission in sour gas flares," *Iranian Journal of Oil and Gas Science and Technology*, vol. 8, no. 1, pp. 1-10, 2019.

[9]   W. Lu *et al.*, "Global proliferation of offshore gas flaring areas," *Journal of Maps*, vol. 16, no. 2, pp. 396-404, 2020. https://doi.org/10.1080/17445647.2020.1762773

[10]   M. Faruolo, T. Lacava, N. Pergola, and V. Tramutoli, "On the potential of the RST-FLARE algorithm for gas flaring characterization from space," *Sensors*, vol. 18, no. 8, p. 2466, 2018. https://doi.org/10.3390/s18082466

[11]   A. Caseiro *et al.*, "Persistent hot spot detection and characterisation using SLSTR," *Remote Sensing*, vol. 10, no. 7, p. 1118, 2018. https://doi.org/10.3390/rs10071118

[12]   E. O. Chukwu, M. O. Faluyi, and I. J. Adaji, "Impact of gas flaring on climate change: A case study ofn Niger delta Region of Nigeria," *Global Scientific Journals*, vol. 9, pp. 1781-1790, 2021.

[13]   L. Uyigue and F. Enujekwu, "Physicochemical analysis of gas flaring impact on the environment of host communities in the Niger-delta," *Journal of Environment Pollution and Human Health*, vol. 5, no. 1, pp. 22-29, 2017.

[14] E. I. Seiyaboh and S. C. Izah, "A Review of impacts of gas flaring on vegetation and water resources in the Niger Delta Region of Nigeria," *International Journal of Economy, Energy and Environment*, vol. 2, no. 4, pp. 48-55, 2017. https://doi.org/10.11648/j.ijeee.20170204.11

[15] A. O. Lawanson, A. M. A. Imevbore, and V. O. Fanimokun, "Effects of waste-gas flares on the surrounding cassava plantations in the Niger Delta Regions of Nigeria," in *Proceedings, Sixth Symposium of the International Society for Tropical Root Crops/hosted by CIP in Lima, Peru, 21-26 February 1983. Lima, Peru: International Potato Center (CIP), 1984*, 1984.

[16] E. Awulu, "Gas flaring in Nigeria: A crisis for the Environment," *Academia Letters*, pp. 1-6, 2021. https://doi.org/10.20935/AL3799

[17] P. Okeke and C. Okpala, "Effects of gas flaring on selected arable soil quality indicators in the Niger Delta, Nigeria," *Sky Journal of Soil Science and Environmental Management*, vol. 3, no. 1, pp. 001-005, 2014.

[18] A. Allam, A. Hamou, D. Mansour, M. Rahila, and A. Dif, "Multi-temporal relationship between surface temperature, land use and normalized vegetation index," *Algerian Journal of Environmental Science and Technology*, vol. 7, no. 3, pp. 2045-2050, 2021.

[19] S. A. Shah, M. Kiran, A. Nazir, and R. Dars, "Evaluation of land surface temperature and normalized difference vegetation index relationship using landsat 8 Satellite images in Mehar Taluka, Dadu," *Pakistan Journal of Geology*, vol. 5, pp. 2521-2915, 2021.

[20] A. A. Bindajam, J. Mallick, S. AlQadhi, C. K. Singh, and H. T. Hang, "Impacts of vegetation and topography on land surface temperature variability over the semi-arid mountain cities of Saudi Arabia," *Atmosphere*, vol. 11, no. 7, p. 762, 2020. https://doi.org/10.3390/atmos11070762

[21] S. Guha, H. Govil, and P. Diwan, "Monitoring LST-NDVI relationship using Premonsoon Landsat datasets," *Advances in Meteorology*, vol. 2020, pp. 1-15, 2020. https://doi.org/10.1155/2020/4539684

[22] M. Fatemi and M. Narangifard, "Monitoring LULC changes and its impact on the LST and NDVI in District 1 of Shiraz City," *Arabian Journal of Geosciences*, vol. 12, no. 4, pp. 1-12, 2019. https://doi.org/10.1007/s12517-019-4259-6

[23] F. Ferrelli, M. A. H. Cisneros, A. L. Delgado, and M. C. Píccolo, "Spatial and temporal analysis of the LST-NDVI relationship for the study of land cover changes and their contribution to urban planning in Monte Hermoso, Argentina," *Geographical Analysis Documents*, vol. 64, no. 1, pp. 25-47, 2018. https://doi.org/10.5565/rev/dag.355

[24] S. Naeem, C. Cao, M. M. Waqar, C. Wei, and B. K. Acharya, "Vegetation role in controlling the ecoenvironmental conditions for sustainable urban environments: A comparison of Beijing and Islamabad," *Journal of Applied Remote Sensing*, vol. 12, no. 1, p. 016013, 2018. https://doi.org/10.1117/1.jrs.12.016013

[25] R. C. Estoque, Y. Murayama, and S. W. Myint, "Effects of landscape composition and pattern on land surface temperature: An urban heat island study in the megacities of Southeast Asia," *Science of the Total Environment*, vol. 577, pp. 349-359, 2017. https://doi.org/10.1016/j.scitotenv.2016.10.195

[26] Z. N. Li, D. Sibo, and T. Bohui, "Review of methods for land surface temperature derived from thermal infrared remotely sensed data," *Journal of Remote Sensing*, vol. 20, pp. 899-920, 2016.

[27] S. Guha, H. Govil, A. K. Taloor, N. Gill, and A. Dey, "Land surface temperature and spectral indices: A seasonal study of Raipur City," *Geodesy and Geodynamics*, vol. 13, no. 1, pp. 72-82, 2022. https://doi.org/10.1016/j.geog.2021.05.002

[28] Y. Ghobadi, B. Pradhan, H. Z. M. Shafri, and K. Kabiri, "Assessment of spatial relationship between land surface temperature and landuse/cover retrieval from multi-temporal remote sensing data in South Karkheh Sub-Basin, Iran," *Arabian Journal of Geosciences*, vol. 8, no. 1, pp. 525-537, 2015. https://doi.org/10.1007/s12517-013-1244-3

[29] USGS, "Landsat 7 and landsat 8 specifications. National Aeronautics and Space Administration [NASA], USA," Retrieved: https://www.usgs.gov/faqs/what-are-band-designations-landsat-satellites. [Accessed 01 July, 2021], 2013.

[30] Google Earth, "Map of Africa showing Nigeria, map of Nigeria and map of Rivers State with the 11 flaring sites examined. Google, USA," Retrieved: https://earth.google.com. [Accessed 3 March, 2022], 2022.

[31] Z. Song *et al.*, "Global land surface temperature influenced by vegetation cover and PM2. 5 from 2001 to 2016," *Remote Sensing*, vol. 10, no. 12, pp. 2034-2044, 2018. https://doi.org/10.3390/rs10122034

[32] S. Huang, L. Tang, J. P. Hupy, Y. Wang, and G. Shao, "A commentary review on the use of normalized difference vegetation index (NDVI) in the era of popular remote sensing," *Journal of Forestry Research*, vol. 32, no. 1, pp. 1-6, 2021. https://doi.org/10.1007/s11676-020-01155-1

[33] S. Guha, H. Govil, A. Dey, and N. Gill, "Analytical study of land surface temperature with NDVI and NDBI using Landsat 8 OLI and TIRS data in Florence and Naples city, Italy," *European Journal of Remote Sensing*, vol. 51, no. 1, pp. 667-678, 2018. https://doi.org/10.1080/22797254.2018.1474494

[34] W. Li, Q. Cao, K. Lang, and J. Wu, "Linking potential heat source and sink to urban heat island: Heterogeneous effects of landscape pattern on land surface temperature," *Science of the Total Environment*, vol. 586, pp. 457-465, 2017. https://doi.org/10.1016/j.scitotenv.2017.01.191

[35] Y. Zhang, I. O. Odeh, and C. Han, "Bi-temporal characterization of land surface temperature in relation to impervious surface area, NDVI and NDBI, using a sub-pixel image analysis," *International Journal of Applied Earth Observation and Geoinformation*, vol. 11, no. 4, pp. 256-264, 2009. https://doi.org/10.1016/j.jag.2009.03.001

[36] A. Berk, G. P. Anderson, and P. K. Acharya, *MODTRAN4 user's manual, air force research laboratory*. North Andover, MA, USA: Ontario Corporation, 1999.

[37] J. A. Barsi, J. R. Schott, F. D. Palluconi, and S. J. Hook, "Validation of a web-based atmospheric correction tool for single thermal band instruments," in *Proceedings of SPIE, Bellingham, WA*, 7, 2005, vol. 5882.

[38] G. Chander and B. Markham, "Revised Landsat-5 TM radiometric calibration procedures and postcalibration dynamic ranges," *IEEE Transactions on Geoscience and Remote Sensing*, vol. 41, no. 11, pp. 2674-2677, 2003. https://doi.org/10.1109/tgrs.2003.818464

[39] C. Zeng *et al.*, "Soil erosion evolution and spatial correlation 1 analysis in a typical karst geomorphology, using RUSLE with GIS," *Solid Earth Discuss*, vol. 8, pp. 721–736, 2017. https://doi.org/10.5194/se-8-721-2017

[40] E. E. Cleland, I. Chuine, A. Menzel, H. A. Mooney, and M. D. Schwartz, "Shifting plant phenology in response to global change," *Trends in Ecology & Evolution*, vol. 22, no. 7, pp. 357-365, 2007. https://doi.org/10.1016/j.tree.2007.04.003

[41] T. Sparks and P. Tryjanowski, "The detection of climate impacts: Some methodological considerations," *International Journal of Climatology: A Journal of the Royal Meteorological Society*, vol. 25, no. 2, pp. 271-277, 2005. https://doi.org/10.1002/joc.1136

[42] V. Dose and A. Menzel, "Bayesian analysis of climate change impacts in phenology," *Global Change Biology*, vol. 10, no. 2, pp. 259-272, 2004. https://doi.org/10.1111/j.1529-8817.2003.00731.x

[43] Y. Deng *et al.*, "Relationship among land surface temperature and LUCC, NDVI in typical karst area," *Scientific Reports*, vol. 8, no. 1, pp. 1-12, 2018. https://doi.org/10.1038/s41598-017-19088-x